Scientific African 26 (2024) e02366

Contents lists available at ScienceDirect

Scientific African

journal homepage: www.elsevier.com/locate/sciaf

Analyzing the spatio-temporal pattern of urban growth and its influence on urban heat islands in the Sekondi-Takoradi metropolis, Ghana

Ernest Biney [a,b,*], Eric Kwabena Forkuo [a,b], Michael Poku-Boansi [c], Kwame O. Hackman [d], Emmanuel Harris [e], Yaw Mensah Asare [b], Daniel Buston Yankey [b], Ernestina Annan [a], Albert Elikplim Agbenorhevi [f]

[a] *WASCAL Graduate Research Programme on Climate Change and Land Use, Department of Civil Engineering, Kwame Nkrumah University of Science and Technology, Kumasi, Ghana*
[b] *Department of Geomatic Engineering, Kwame Nkrumah University of Science and Technology, University Post Office Box PMB, Kumasi, Ghana*
[c] *Department of Planning, Kwame Nkrumah University of Science and Technology, Kumasi, Ghana*
[d] *Data Management Department, WASCAL Competence Center, Ouagadougou, Burkina Faso*
[e] *Department of Statistics and Actuarial Science, Kwame Nkrumah University of Science and Technology, University Post Office Box PMB, Kumasi, Ghana*
[f] *WASCAL Climate Change and Water Resources, Universite d'Abomey-Calavi, Benin*

ARTICLE INFO

Editor: DR B Gyampoh

Keywords:
Normalized Difference Vegetation Index (NDVI)
Urban Thermal Field Variance Index (UTFVI)
Sekondi-Takoradi
Land Surface Temperature (LST)
Urban Heat Island (UHI)
Normalized difference built-up index (NDBI)

ABSTRACT

The rapid urbanization in Sekondi-Takoradi, Ghana has significantly transformed the land cover, resulting in the proliferation of impervious surfaces and a decline in vegetation. However, the influence of this urban growth on the development of urban heat islands (UHIs) in the metropolis remains understudied. This study aimed to fill this research gap by employing Landsat images to explore the influence of urban growth on urban heat islands in the metropolis from 1991 to 2023. The supervised random forest technique was utilized to map the land cover changes. Furthermore, the computed normalized difference built-up index (NDBI), normalized difference vegetation index (NDVI), land surface temperature (LST), and urban thermal field variance index (UTFVI) were used to analyze the influence of urban expansion on UHIs. The findings revealed a 63.07 km^2 increase in built-up areas and a 60.99 km^2 decrease in vegetation cover during the study period. This dramatic land use change led to a 3.1°C rise in mean LST and a 19.38 km^2 expansion of areas affected by the UHI effect. The UTFVI analysis further indicated a 33.63 km^2 increase in the worst ecological zone due to the temperature rise. Statistical analysis between LST, NDVI, and NDBI revealed significant variability in explaining the intensity of LST and UHI in the metropolis over the study period. The study equips city authorities and planners with the fundamental knowledge needed to prepare a sustainable development plan that alleviates adverse effects of urban growth and elevated temperature-related issues. Also, the findings contribute to the global efforts in promoting more livable and climate-resilient urban environments.

* Corresponding author.
E-mail address: ernest_biney@yahoo.com (E. Biney).

https://doi.org/10.1016/j.sciaf.2024.e02366
Received 17 May 2024; Received in revised form 8 August 2024; Accepted 13 September 2024
Available online 15 September 2024

Introduction

Over the past few decades, the world has experienced speedy urban growth with the majority of this increase taking place in developing nations, particularly in Africa. Unfortunately, this speedy urban growth is significantly changing the land cover and the biophysical environment into impervious surfaces [1,2]. According to Kumi-Boateng and Stemn [3], urban growth is recognized as a major and enduring type of land use land cover change with significant ecological consequences, and the extent to which it has increased is correlated with population growth and economic development. Halder and Bandyopadhyay [4] also pointed out that urban growth alters the natural landscape by replacing it with impermeable surfaces which significantly impacts local weather and climate. Per the research of Jumari et al. [5], there has been a global increase in the surface temperature by 1.53 ℃ due to the drastic rise in urbanization. Rapid urbanization significantly impacts the thermal environments of cities by transforming the natural surfaces into built-up areas [6]. Urban areas have a higher tendency to absorb solar radiation and retain heat due to the presence of artificial structures and impervious materials like buildings, asphalt, paved surfaces, and metals. These materials store heat during the day and release it at night due to their greater thermal conductivity and capacity [7]. Therefore, a dense concentration of these artificial structures coupled with a lack of green spaces creates "islands" with elevated temperatures [8]. Dutta [9] and Sekertekin and Bonafoni, [10] assert that replacing natural cover types with impermeable materials modifies the surface energy balance of the earth and subsequently increases land surface temperature[1] (LST). This causes a warmer climate in urban areas than the surrounding rural environment, bringing about a phenomenon known as urban heat island (UHI) [11]. Mostly, UHI areas exhibit higher LST [12]. Urban geometry, construction materials, and changes in land cover are the main causes of UHI [12]. The presence of dark materials and heat-absorbing impermeable surfaces make UHI predominant in built-up areas [13]. Potentially, the rise in UHI leads to changes in precipitation patterns, increased demand for energy and air conditioners, and elevated pollution levels which contribute to global warming and negatively impact environmental quality [14]. Zhao et al., [15] noted that a significant UHI effect affects the comfort and health of urban residents and impedes further improvements in the quality of life and the city's development. In light of this, the United Nations (2018) predicts that by 2050 the trend of LST and dangerous pollutants in urban air will affect about 68 % of the global population [16]. Several research studies have established thermal comfort indicators to quantify the impact of UHI intensity [17]. Due to the strong correlation of the urban thermal field variance index (UTFVI) with LST, it has become the preferred and widely used index for the ecological assessment of the urban environment [18]. Also, UTFVI does not require parameter datasets like humidity and wind speed, which are demanded by other comfort indicators but are not readily accessible in high spatial resolution for most areas including the study area. Importantly, the UTFVI has been examined with Landsat data and shown satisfactory results [19]

Throughout the preceding years, Ghana has witnessed substantial expansion in its urban populace. For instance, from 1931 to 2010, the urban population increased from 9.4 % to 50 % [20] and today, approximately 15.5 million out of the 30 million Ghanaian population which represents 58 % reside in urban centers [21]. Also, there has been an increase in Ghana's urban centers to 212 urban centers (https://africapolis.org/en/country-report/Ghana; [21]). This evidence of urban growth is rapidly changing the land use land cover pattern in Ghana into built-up. According to Jumari et al., [5], a contributory factor to the climate change phenomenon is the transformations in land use land cover. Sadly, Sekondi-Takoradi, which is one of Ghana's urbanized metropolises in the western region is no exception to the increasing loss of land cover to impervious surfaces. According to the Ghana Statistical Service [21], the urbanization rate in the metropolis was approximately 61.8 % as of 2021 which represents a significant increase from 36.4 % in 1984. The prime cause of rapid urban growth in the metropolis is due to the concentration of economic activities and industries within the metropolis [22]. As of 2021, cement and concrete made up 75.7 % of the construction materials used in the metropolis for outer walls while wood made up 4.7 % of the main construction materials for outer walls. Also, the main construction materials for roofs within the metropolis were metal sheets (56.9 %), slate or Asbestos (25.0 %), and cement or concrete (12.3 %). These building materials are mostly impermeable and have significant heat retention capacity which influences the natural ecology and local climate ecology of an area. In some regions of Ghana, especially in the Greater Accra region, UHI has been extensively addressed [7,20]. However, to the best of the authors' knowledge, the only studies on urban heat islands carried out in the Sekondi-Takoradi metropolis was conducted by Kumi-boateng and Stemn [3]. Kumi-Boateng and Stemn [3] examined the impact of urban expansion on the thermal environment in the Sekondi-Takoradi metropolis, but the analysis only spanned a brief period of 17 (1991-2008), data was limited to only Landsat 5 and 7 and lacked information on the extent, intensity and magnitude of UHI which is covered extensively in this study. Also, using the urban thermal field variance index (UTFVI) to measure the thermal comfort level of the metropolis was not addressed in the works of Kumi-Boateng and Stemn [3]. Even taking Ghana as a whole, less attention has been given to the application of UTFVI in UHI studies. This study addresses the research gap by incorporating UTFVI to analyze UHI and provides information on the extent, intensity, and magnitude of UHI which is lacking. Providing such detailed information on UHI in one of Ghana's most urbanized metropolises will help to facilitate planning and regulate unplanned development in the area. Furthermore, Guha et al., [18] demonstrated that LST corresponds variably with seasons and surface cover, so, it cannot accurately and universally depict the same situation everywhere. This stems from the fact that every city has a distinctive nature and their complex interplay of factors affects LST. As a result, Kursah, [19] has explicitly emphasized the need for location-specific studies on LST to develop a comprehensive universal understanding of how urban growth influences heat patterns.

The application of RS and GIS technologies has witnessed significant growth in assessing land use land cover (LULC) changes and LST variations in urban areas. These technologies have garnered considerable interest in studying ecosystem transformations, biodiversity, and global climate patterns. Traditional methods of change detection in LULC scenarios and direct field visits for LST monitoring are resource-intensive, time-consuming, and susceptible to errors. However, by integrating RS and GIS technologies, it becomes more efficient to evaluate, monitor, and model

[1] LST refers to the radiant energy emitted at a maximum distance of 1.2m above the earth's surface from diverse materials that absorb and release heat [7].

changes in LULC, urban growth, and UHI [16,23]. Extensive studies have utilized RS and GIS to discern the thermal characteristics of urban surfaces and established connections between the various LULC classes and the LST in various ways. For instance, Wemegah et al., [20] evaluated the phenomenon of urban heat island warming in the Greater Accra region using land cover types, thermal data, and daily observed minimum and maximum temperature data. Stemn and Kumi, [24] used land surface temperature to model heat-related conditions in the Wassa West mining area of Ghana. Jahan and Rahman, [23] used remote sensing and GIS to simulate surface temperature under climate change scenarios. Huda and Al, [25] employed remote sensing and statistical techniques to evaluate the relationship between Land Surface temperature and land cover in Chattogram City. Kumi-Boateng and Stemn [3], integrated RS and GIS to evaluate the impact of rapid urban growth on surface temperature. By combining GIS with RS, this study carried out a thorough evaluation of UHI warming in the Sekondi-Takoradi Metropolis. Specifically, the study: (1) analyzed the pattern of land use land cover within the metropolis; (2) assessed the spatiotemporal distribution of Land Surface Temperature (LST) and Urban Heat Island (UHI) within the metropolis; (3) established a relationship between UHI and urban development by examining the correlation between NDVI, NDBI, and LST; (4) evaluated the thermal comfort level of the metropolis based on UTFVI. Achieving these research objectives offers valuable insights for urban planners and city authorities, equipping them with the essential knowledge to develop sustainable development plans that mitigate the adverse effects of urban growth and elevated temperatures in the Sekondi-Takoradi metropolis. Furthermore, the findings contribute to global efforts to create more livable and climate-resilient urban environments. This research is organized as follows: 1. Introduction 2. Materials and methods 3. Result and discussion 4. Conclusion.

Materials and methods

The following subsections discuss the materials and methods (Fig. 1) employed in the study.

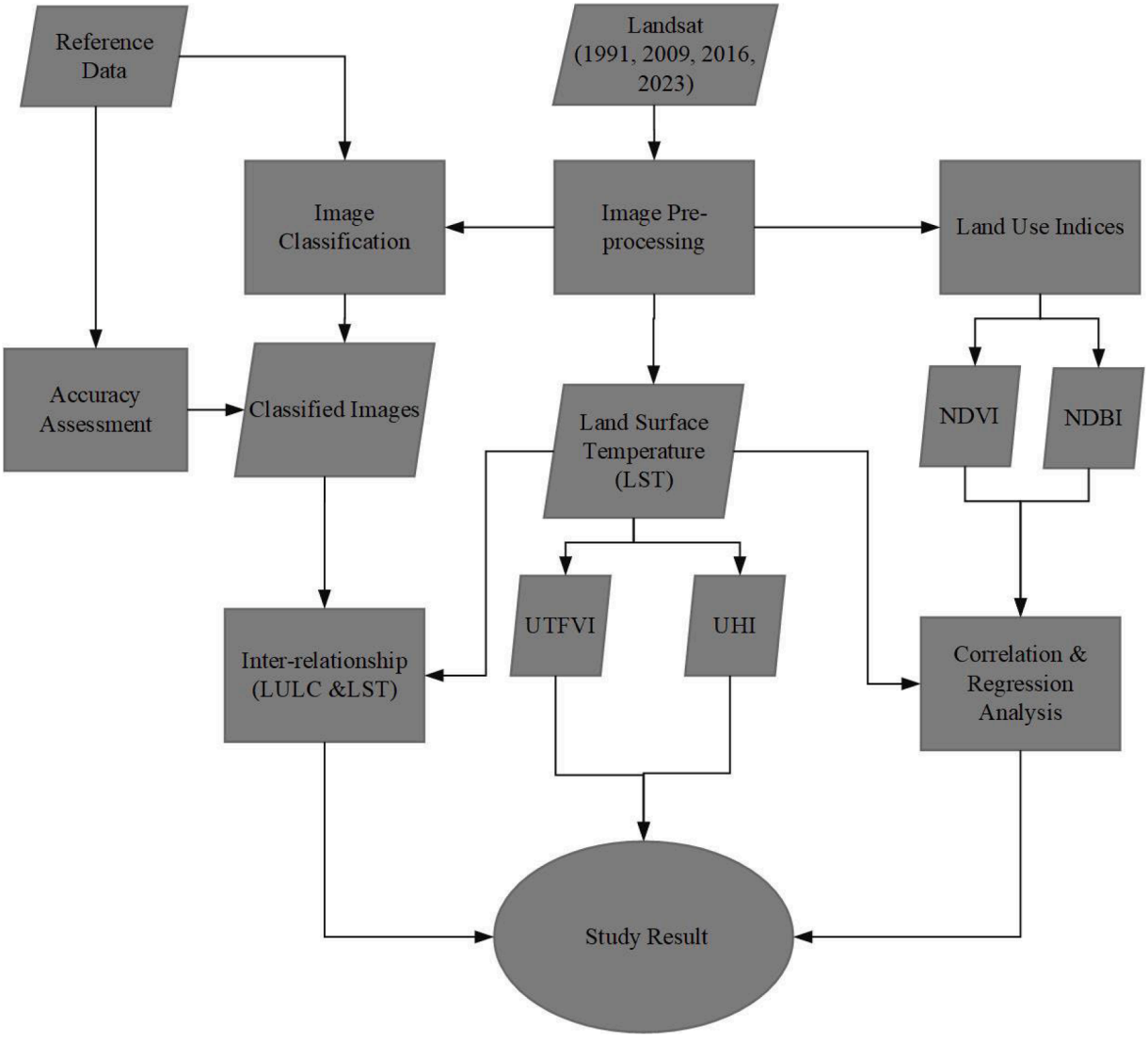

Fig. 1. the methodical workflow of the study.

Study area

As illustrated in Fig. 2, Sekondi-Takoradi is located at latitude 4° 52′ 30″ N and 5 °04′ 00″ N and longitudes 1° 37′ 00″ W and 1° 52′ 30″W. It is the administrative hub for the western region of Ghana with a land area of 191.7 km^2. 96.1 % of the population in the metropolis resides in urban areas, while 3.9 % resides in rural areas. This demonstrates that a significant portion of the city residents reside in urban regions [26]. Due to the role of the metropolis as a commercial and industrial hub, it draws immigrants from all walks of life. The population of the metropolis has increased from 559,548 in 2010 to 1,120,000 by the year 2021 [21,27,28]. It has an equatorial climate and an average yearly temperature of 22°C. Rainfall in the metropolis occurs in two distinct seasons: the major season starts from March to July and the minor season lasts from August to November. According to Aduah et al., [29], the average annual rainfall is 1380 mm or 122 rainy days. The study area was chosen because it hosts various construction enterprises and industries. These enterprises and industries engage in burning fossil fuels for manufacturing, energy production, industrial processes, and transportation which are key contributors to elevated temperatures. Therefore, it is imperative to conduct LST and UHI analysis to effectively monitor the temperature dynamics in Sekondi-Takoradi. Also, vegetation, which acts as a heat sink for the metropolis is massively degrading and this renders the metropolis vulnerable to severe thermal conditions [30].

Dataset used

Details of the datasets employed in this study are presented in Table 1. To avoid the problem of phenology which can affect the accuracies of the study as well as limit the impact of the different seasons on land surface changes, the images were chosen at the same season.

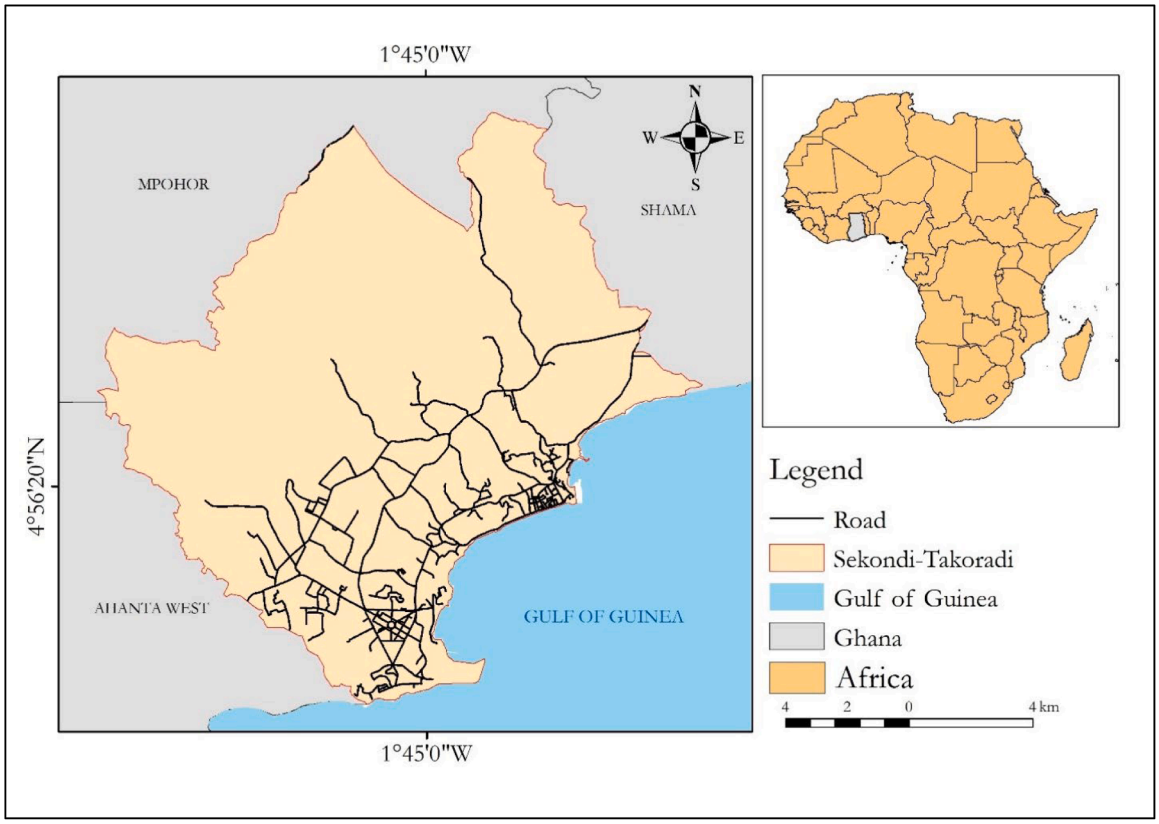

Fig. 2. Study area.

Table 1
Dataset used.

Sensor	Source	Path/Row	Resolution	Acquisition date
Landsat 5 (TM)	USGS earthexplorer	194/57	30m	01/01/1991
Landsat 7 (ETM+)	USGS earthexplorer	194/57	30m	01/02/2009
Landsat 7 (ETM+)	USGS earthexplorer	194/57	30m	06/01/2016
Landsat 8 (OLI/TIRS)	USGS earthexplorer	194/57	30m	01/01/2023
GPS data	Field survey	NA	3m	
Shapefile and other vector data	Survey Department of Lands Commission	NA		
NA	NA			

Methods

This section concisely describes the analysis undertaken for the study as shown in Fig. 1.

Image pre-processing and classification

Satellite images are commonly affected by distortions during the process of imaging and so need to be corrected before any further processing and analysis can be applied [31]. In this study, radiometric and geometric corrections were applied to the acquired Landsat images using QGIS software. Several classification algorithms such as the maximum likelihood classifier (MLC), support vector machine (SVM), and random forest (RF) have been used in mapping out land cover types. The supervised random forest method was used to classify the images into three classes (Table 2). This algorithm was chosen due to its enhanced ability to handle outliers and data noise [32], superior performance with multi-dimensional datasets from various sources, faster processing time, and higher accuracy compared to classifiers like Maximum Likelihood, Support Vector Machine, and Kernel Neural Network [33]. Additionally, its reliable classification outcomes have led many studies to recognize random forest as an effective land use land cover classifier [31]. Fernández-Delgado [34] demonstrated this by evaluating 179 classifiers from 17 families using 121 datasets, finding random forest to be the best. Furthermore, random forest can manage missing values, categorical, and unbalanced data—capabilities not present in SVM [35,36].

Accuracy assessment

According to Khwarahm et al., [37], classified images must be assessed for reliability after a classification process. This is because misclassified images will have a negative influence on the outcome of a study [38]. Using reference data, the classified images were assessed of their accuracies. The stratified random sampling point technique was used to sample 300 points for each classified image to create an error matrix. The error matrix is a composition of producer accuracy (PA), User accuracy (UA), Overall accuracy, (OA), and Kappa coefficients (KC). Eqs. (1)-(4) were respectively used to estimate PA, UA, OA, and KC [39,40]. The ArcGIS 10.5 was used to perform the accuracy assessment

$$Overall\ accuracy = \frac{Total\ number\ of\ correctly\ classified\ pixels}{Total\ number\ of\ reference\ pixels} \times 100 \tag{1}$$

$$User\ accuracy = \frac{Corrected\ classified\ pixels\ in\ each\ class}{Total\ classified\ pixel\ in\ that\ class\ (row\ total)} \times 100 \tag{2}$$

$$Producer\ accuracy = \frac{Corrected\ classified\ pixels\ in\ each\ class}{Total\ classified\ pixel\ in\ that\ class\ (the\ column\ total)} \times 100 \tag{3}$$

$$Kappa\ Coefficient = \frac{(total\ accuracy - random\ accuracy)}{(1 - random\ accuracy)} \tag{4}$$

Land use indices

Two distinct indices related to land use were estimated. These indices are the normalized difference vegetation index (NDVI) and normalized difference built-up index (NDBI). NDVI is an essential indicator of urban climate [31]. It is widely used to assess the quantity and health of vegetation in an area. Its values range from +1 to -1, with large positive values representing vegetation, negative values indicating water, and 0 denoting built-up or bare land [41]. Using Eq. (5), the NDVI of the study area was computed [40].

Table 2
Description of class types.

Class type	Description
Water	Lakes, rivers, streams, ponds, wetlands, lagoons, all in-land water bodies.
Vegetation	Areas with grass, farmland, forest, and agricultural land.
Built-up	Impervious surfaces, man-made structures, settlement.

$$NDVI = \frac{NIR - RED}{NIR + RED} \tag{5}$$

Where NIR denotes Near-Infrared.

NDBI is also commonly used to retrieve information about the imperviousness of an area. It also ranges between the values +1 to -1 where water, vegetation, and built-up are denoted respectively by zero, negative, and positive values. As an important indicator of urban climate, the NDBI was computed using Eq. (6) [31,40].

$$NDBI = \frac{MIR - NIR}{MIR + NIR} \tag{6}$$

Where MIR denotes mid-infrared and NIR denotes Near-Infrared.

Derivation of land surface temperature (LST)

According to Al-Kafy et al., [16], the thermal bands of Landsat stores temperature data as digital numbers. Therefore, using the thermal bands of various Landsat imageries, the surface temperature can be determined. Band 6 is the thermal band for Landsat 5 and 7 whereas bands 10 and 11 are the thermal bands for Landsat 8 [25]. Concerning the thermal band of Landsat 8, Al-khakani [42], recommended using band 10 for LST estimation due to the considerable uncertainties associated with band 11. Following this recommendation, this study adopted band 10 and band 6 for the LST estimation. The derivation of LST from Landsat 5 and 7 followed a 3-step process (Fig. 3) while LST from Landsat 8 was obtained using a 5-step process (Fig. 4). These steps are widely known and efficiently used to determine LST [7].

Mapping out Urban Heat Islands (UHIs) and Urban Thermal Field Variance (UTFVI)

The UHI zones were determined by applying the following equations [43,44].

$$\text{LST} > \mu + 0.5{*}\delta \text{ referred to UHI zones} \tag{7}$$

$$0 < \text{LST} \leq \mu + 0.5 * \delta \text{ referred to non UHI zones} \tag{8}$$

where μ represents the mean and δ represents the standard deviation of the LST.

Due to the variations in the years and the diverse atmospheric conditions that affect satellite images, it is not suitable to directly compare satellite images from different years. To ensure a valid comparison, the images were normalized using Zhang's proposed Eq. (9) [25].

$$SUHI = \frac{T_s - T_m}{STD} \tag{9}$$

From Eq. (9), T_S denotes the land surface temperature, T_m represents the average LST, and STD refers to the standard deviation. In light of the UHI values, the study area was categorized into areas with UHI impact and areas without UHI effect. To quantitatively

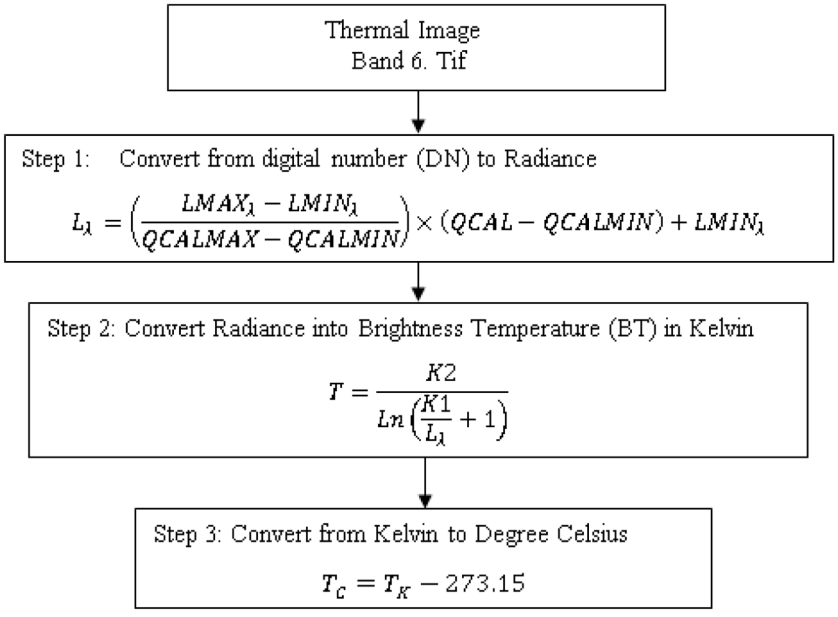

Fig. 3. A 3-step method for deriving LST from the Landsat 5 and 7.

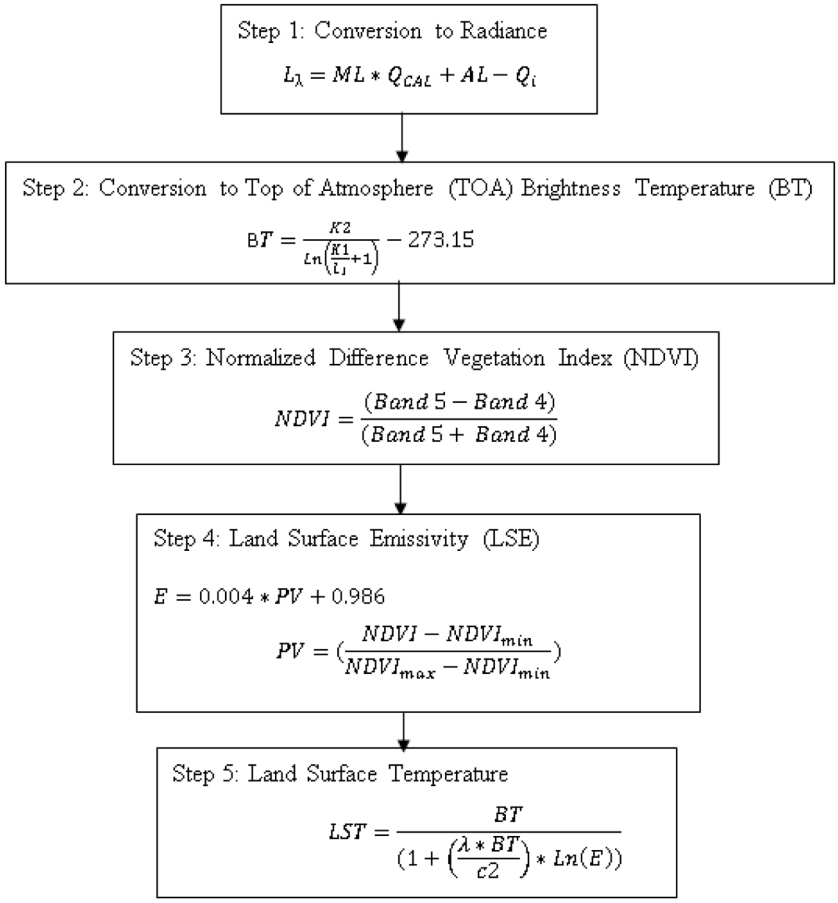

Fig. 4. A 5-step method for deriving LST from Landsat 8.

explain the UHI sensitivity, UTFVI, as expressed in Eq. (10) was applied [20,25].

$$UTFVI = \frac{T_s - T_m}{T_s} \tag{10}$$

Where T_s denotes the LST of the area, T_m is the average LST. Based on the UTFVI, the study area was further divided into six distinct classes [20,41]. These UTFVI classes are matched with an ecological evaluation index (EEI) (Table 3). The ecological evaluation index is a metric that measures the influence of urban thermals on urban ecological life [25].

Result and discussion

The results of the analysis conducted in this study are thoroughly presented and discussed in sub-themes under this section.

Land use land cover classification and accuracy assessment

Observing from Fig. 5, a significant transformation can be seen in the land use land cover pattern of the study area over the period.

Table 3
Threshold values of UTFVI and its ecological evaluation index (EEI).

UTFVI range	UHI Effect type	EEI
<0	None	Excellent
0-0.005	Weak	Good
0.005-0.010	Middle	Normal
0.010-0.015	Strong	Bad
0.015-0.020	Stronger	Worse
>0.020	Strongest	Worst

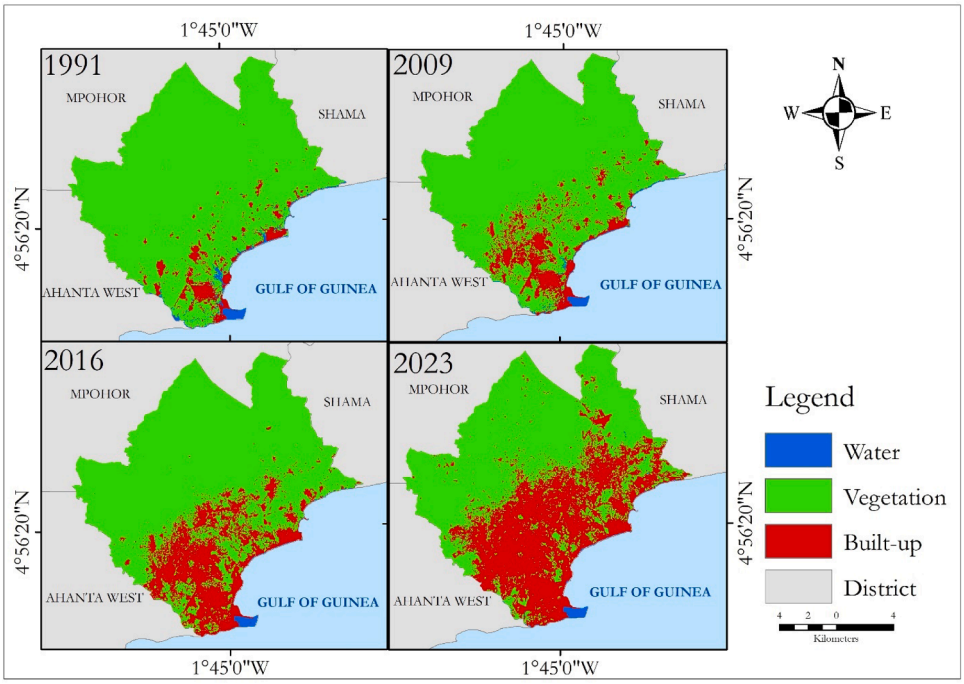

Fig. 5. LULC map from 1991 to 2023.

These changes are statistically detailed in Table 4.

Water displayed a dynamic and contrasting pattern across the four-time steps. From 1991 to 2016, water declined drastically by 2.3 km^2 but increased slightly by 0.27 km^2 between 2016 and 2023 (Table 4). The decline in water is possibly due to the expansion of built-up (Table 4), a shift in hydrological dynamics, and sedimentation [45]. According to Mensah et al., [46], the reduction of water could be explained by the significant decrease in the water retention capacity in watershed and wetland areas due to land degradation and loss of vegetation as seen in Table 4. In addition, Muruganandam, (2023) expresses that the reduction in water level can be attributed to climate change as it causes changes in rainfall patterns and hydrological cycles. This has been proven in the works of Huber (2024), as climate change has led to the depletion of glaciers, consequently affecting water availability directly or indirectly. However, the slight increase in water could be attributed to the occurrence of floods and natural changes in water level [47]. The cumulative decrease in water over the study period indicates the dynamic nature of aquatic ecosystems in the metropolis and its vulnerability to changes in the environment. Vegetation experienced a continuous decline in its coverage throughout the time steps of the study period. From Table 4, a substantial reduction of 10.4 km^2 occurred between 1991 and 2009 and a decrease of 15.66 km^2 and 34.93 km^2 from 2009 to 2016 and 2016 to 2023 respectively. These changes are explained mainly by built-up expansion (Table 4; [47]), and other factors such as deforestation [48], ecological changes, and land use practices [49]. Although the rate of reduction has not been uniform, the significant overall decline of 60.99 km^2 indicates the intricate relationship between urbanization, land management, and environmental conversation (Nyamekye, 2020; Younes, 2023). The spatial coverage of built-up progressively expanded throughout the study period at a cumulative amount of 63.07 km^2. This consistent growth reflects developmental initiatives, urbanization trends, migration patterns, and population growth in the metropolis [45]. Among the transitional years, a significant surge of 34.65 km^2 was observed between 2016 and 2023, which highlights the increasing conversion of natural space into built-up spaces and the concurrent infrastructure development in the metropolis. Hence, indicates the rate at which the metropolis is becoming urbanized and the possible presence of unplanned built-up. As a result, Khan et al., [39] recommend the implementation of strategies and initiatives that will check unauthorized urban growth and inappropriate conversion of natural space or water and vegetation into built-up. The rise in built-up at the cost of other land covers is in line with the work of Asare et al., [50], Biney & Boakye [51], and Wemegah et al., [20].

Table 4
Area coverage of land cover classes.

	km^2				%			
LULC	1991	2009	2016	2023	1991	2009	2016	2023
Vegetation	177.72	167.32	151.66	116.73	92.72	87.29	79.13	60.90
Built-up	10.56	22.13	38.98	73.63	5.51	11.55	20.33	38.42
Water	3.38	2.21	1.03	1.30	1.77	1.16	0.54	0.68
Total	191.66	191.66	191.66	191.66	100	100	100	100

Generally, the analysis of the land use land cover revealed a persistent expansion in built-up, a slight fluctuation in water, and a significant decrease in vegetation. These changes reflect the complex interplay of urbanization, economic development, environmental conservation, and natural land dynamics in the metropolis over the study period.

Accuracy Assessment

According to Obeng et al., [52], image classification is considered reliable for analysis if its overall accuracy is above 85 % and kappa statistics is above 0.7. From Table 5, the accuracy values were above the standardized criteria proposed by Obeng et al., [52], hence, an indication of good classification.

Analysis of land use indices

From Fig. 6, the highest NDVI value was recorded in 1991 while the lowest NDVI value was recorded in 2009. Although most of the NDVI values are positive, they are closer to zero than +1, indicating significant urbanization in the metropolis. Consequently, built-up areas have expanded considerably in the metropolis over the studied period.

NDBI, however, revealed a persistent increase throughout the study period (Fig. 7). At each time point, the highest NDBI values were consistently observed in the southern-western and central regions of the study area, attributed to the presence of dense built-up areas. Conversely, the lowest NDBI values were identified in the northern and eastern areas due to the prevalence of high-density vegetation cover. This observed rise in NDBI values demonstrates a positive association with elevated LST readings, implying a direct correlation between the density of built-up areas and surface temperature as illustrated in Fig. 8.

Table 5
Accuracy assessment result.

Class	User Accuracy				Producer Accuracy			
	1991	2009	2016	2023	1991	2009	2016	2023
Water	86.00	90.00	95.00	97.00	88.66	91.84	94.06	96.04
Vegetation	89.00	93.00	96.00	98.00	86.41	87.74	93.20	94.23
Built-up	88.00	100	93.00	93.00	88.00	92.71	96.88	97.89
Overall accuracy (%)	87.67	90.67	94.67	96.00				
Kappa Coefficient	0.82	0.86	0.92	0.94				

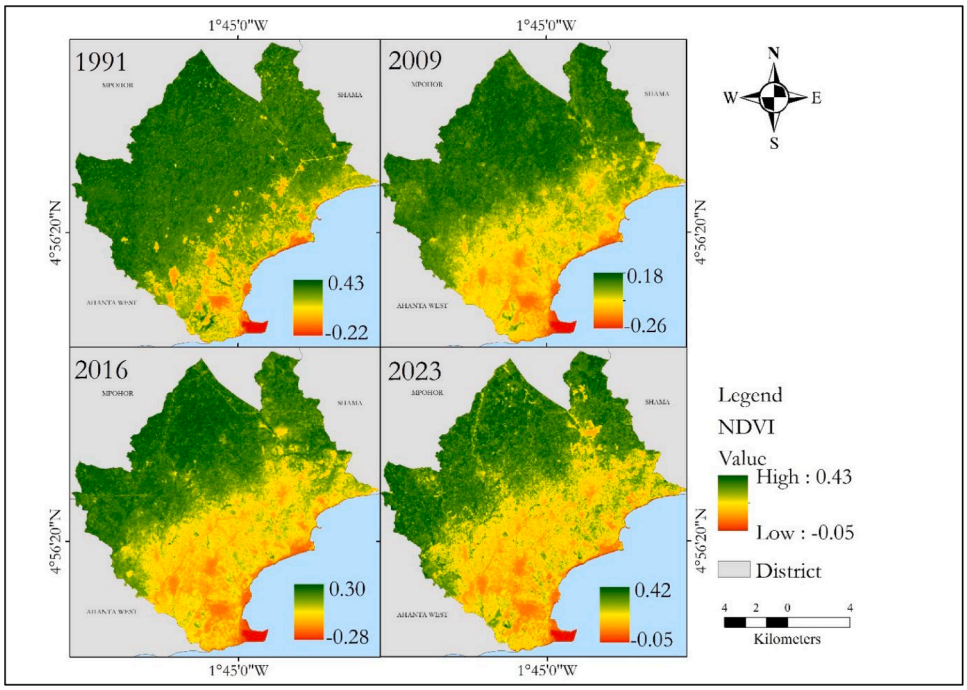

Fig. 6. NDVI map.

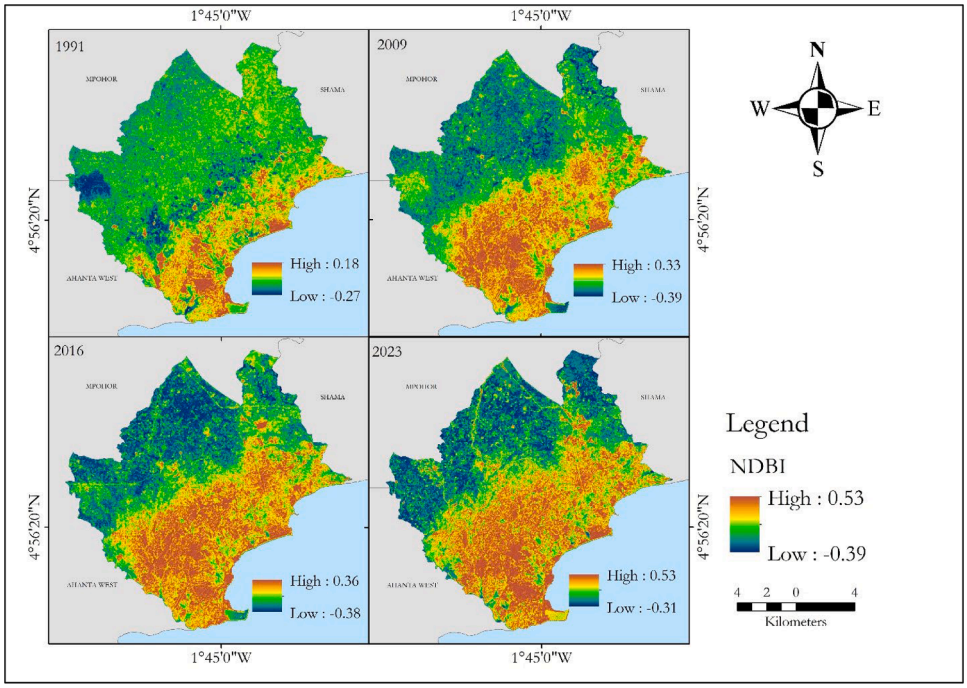

Fig. 7. NDBI map.

Analysis of land surface temperature (LST).

Advanced remote sensing methods and thermal sensors have facilitated convenient observation and measurement of land surface temperature which was previously challenging to perceive with the real eyes [53]. Therefore, by using thermal bands from Landsat imagery, LST for the years 1991, 2009, 2016, and 2023 was assessed (Fig. 8). These maps were color-symbolized with shades ranging from yellow to dark brown to represent low to high temperatures. By visually comparing the LST maps, it is evident that areas with high LST have expanded over the years, signifying an increase in high-temperature areas by 2023. Also, low temperatures were recorded in the northern part due to the presence of significant vegetation cover. The southern and central regions had high temperatures due to the increase in built-up and reduced vegetation. Thus, the varying land cover across the study area influenced the surface temperature. This outcome is consistent with the findings of Negesse et al., (2024) who found that the patterns in LST are closely correlated with the thermal properties of different land cover. Additionally, Ullah et al., (2024) revealed that differences in surface illumination due to irregular landscapes also influence the variability in LST. Hence, landscape structure, land cover, urban sprawl, and geographic features have been identified as influencing factors of LST (Ghanbari et al., 2023).

Statistically, the mean LST showed variations over the years (Fig. 9). It increased by 3.1°C over the entire period and this indicates that the mean LST increased by 1.03°C every 10 years. This increase of 3.1°C is in line with the predictions made by Rasul et al. [54] which indicates a global increase in land surface temperature by 1.40°C to 5.80°C by the 21st century. Similarly, the IPCC's prediction of an increase in global surface warming between 1.1°C and 6.4°C along with increasing heat waves and hot extremes by the 21st century aligns with this study's findings (Aflaki et al., 2017). Moreover, the mean values are close to the annual average temperature range of 22°C to 28°C [19]. Stemn & Kumi, [24], also, reported an increase in the mean LST in the Wassa West Mining area from 1990 to 2020. Further, the increase in the minimum and maximum LST by 1.4°C and 4.3°C, respectively is closely linked to the decline in vegetation and water [29]. However, Badasa et al., [55], assert that surface temperature is expected to increase due to global warming.

Area distribution of LST over the study period

The LST for the various years was broadly categorized into low-temperature class (18-21°C and 21-24°C) and high-temperature class (24-27°C, 27-30°C, and >30°C) and the area of the classes computed (Table 6). LST in 1991 occupied an area of 54.27 km^2 for the low-temperature class whereas the high-temperature class occupied an area of 137.39 km^2. In 2009, the low-temperature class occupied an area of 184.66 km^2 and the high-temperature class occupied an area of 5.96 km^2. Further, in the year 2016, the low surface temperature class covered an area of 148.69 km^2 and the high-temperature class also increased to 42.24 km^2. Ultimately, in the year 2023, the surface temperature occurred within three classes. However, there existed significant differences in the type of class and the respective area covered by each temperature class. All temperature values for 2023 fell within the high-temperature class with extreme temperatures (>30°C) recorded only in 2023. This observed phenomenon substantiates the temporal increase in LST in the study area over time. Moreover, findings from Table 6 showed an increase in the dispersion and intensity of urban heat islands, which poses

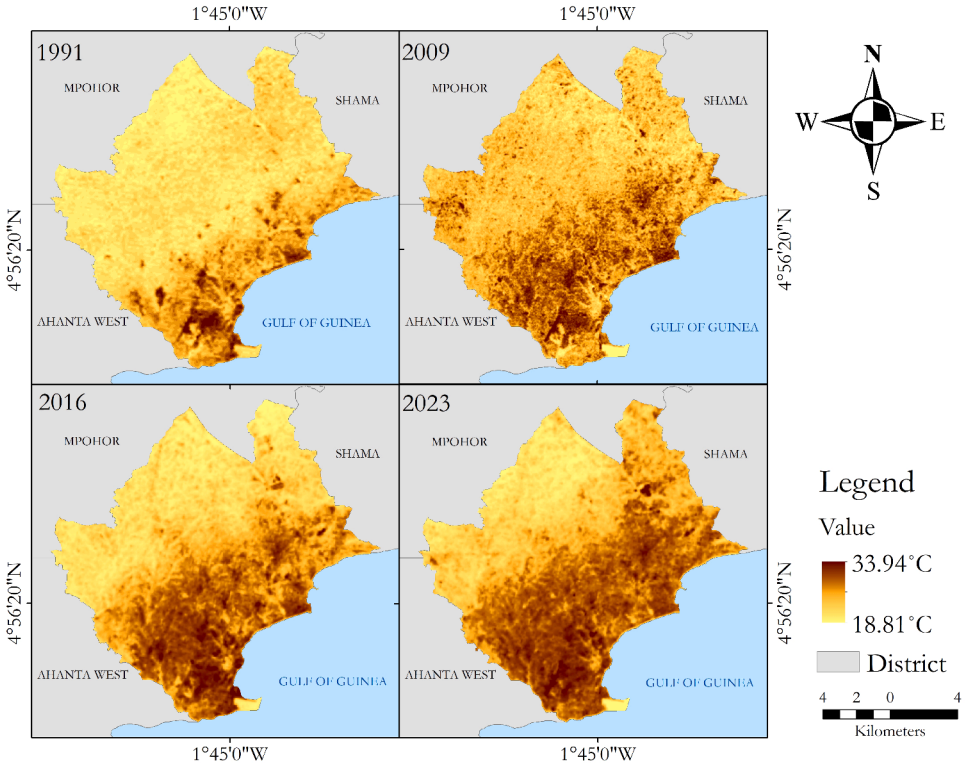

Fig. 8. LST map of the metropolis.

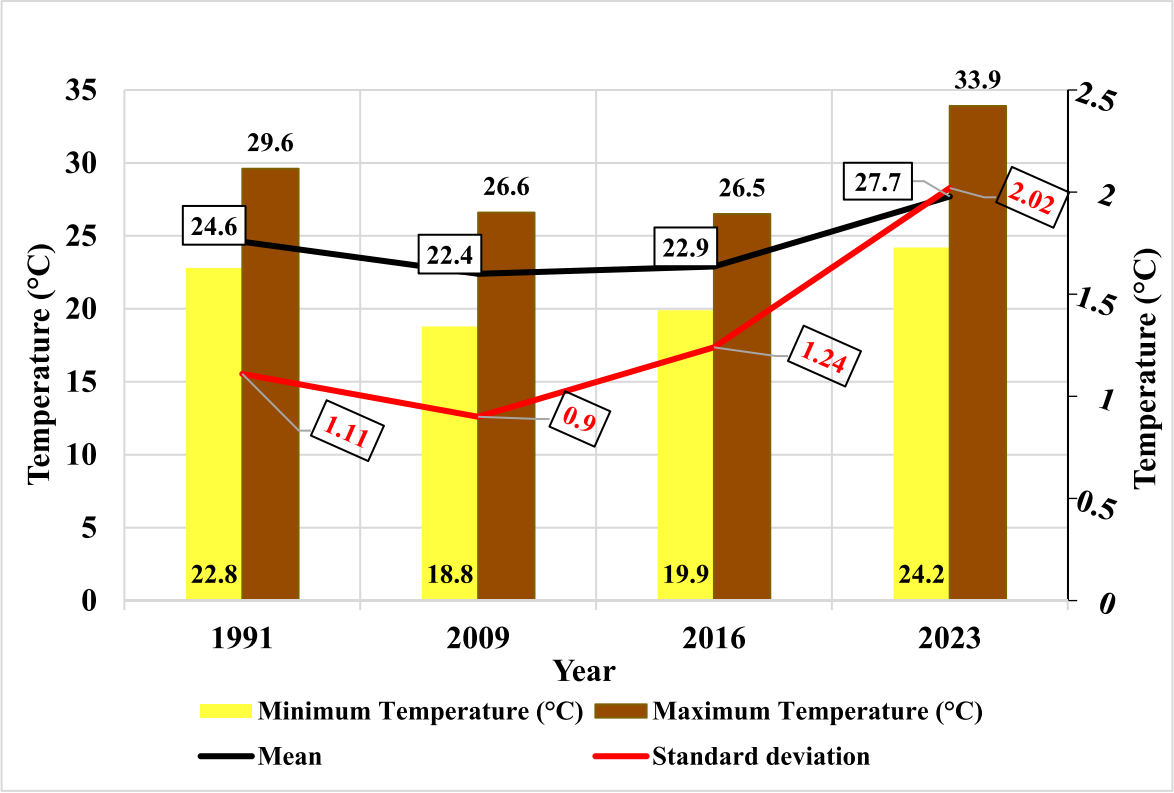

Fig. 9. Graphical analysis of LST trends.

Table 6
The areas associated with the LST class.

Year	Total Area (km^2)	LST classes in km^2 and %				
		18-21°C (1)	*21-24°C (2)*	*24-27°C (3)*	*27-30°C (4)*	*>30°C (5)*
1991	191.66	0.00(0.00)	54.27 (28.31)	130.68(68.18)	6.71(3.50)	0.00(0.00)
2009	191.66	5.96 (3.11)	178.70(93.24)	7.00(3.65)	0.00(0.00)	0.00(0.00)
2016	191.66	14.69(7.67)	134(70.20)	42.42(22.13)	0.00(0.00)	0.00(0.00)
2023	191.66	0.00(0.00)	0.00(0.00)	82.24(42.91)	76.69(40.01)	32.73(17.08)

significant challenges. Addressing these challenges demands urgent consideration from local authorities, urban planners, and policymakers, as emphasized in the works of Badasa et al. [55] and Stemn and Kumi [24].

UHI and UTFVI

The UTFVI and areas with and without UHI effects are statistically highlighted in Table 7. From 1991 to 2023, the UHI threshold rose considerably by 13.55°C. This was accompanied by a 10.14 % increase in areas with UHI effects, at the expense of areas without UHI effects. These findings align with recent research results of Wemegah et al., [20], Huda and Al [25], and Siddique et al. [56] in the cities of Accra, Chattogram, and Beijing respectively. As noted by Kursah [19], increased UHI can directly induce physiological stress in humans and accelerate the risks of morbidity and mortality for the population.

Further, the UTFVI values revealed a decrease in the excellent zone from 67.02 % in 1991 to 50.76 % in 2023 (Table 7). This zone consists of areas where water and green spaces are abundant. Mainly, the northern, pockets of the central and southern-eastern parts experienced excellent thermal conditions This aligns with the findings of Guha, [41] where regions with high levels of vegetation and water bodies experienced excellent thermal conditions. Conversely, 26.30 % of the study area under "worst zone" in 1991 increased to 42.19 % in 2023. This category encompasses the southern-western sector (Fig. 10), primarily characterized by impervious surfaces and urban development. Despite the closeness of the study area to the coastline, it showed high UTFVI. This demonstrates how anthropogenic activities have greater influence on the study's thermal environment than natural forces. It also aligns with the finding that human activities have a greater impact on the formation of UHI than natural factors [57]. For instance, the fishing communities and the harbor experienced the worst thermal conditions due to the high rate of heat-generating activities such as smoking of fish, burning fossil fuels, and pollution emissions from the cement factory, vehicles, and anchored vessels at the port. These activities have the potential to trap returning radiation, warm the surfaces, and increase the mean LST [18]. In view of this, Kursah, [19] suggests using afforestation techniques to turn urban areas into green spaces. Guha, (2023) revealed that zones with excellent thermal comfort increased after the implementation of mitigation programmes in Raipur City. The "normal" thermal condition is observed in patches surrounding the areas exhibiting excellent thermal conditions, while, the bad, and worse, conditions are prevalent in proximity to areas marked by extensive built-up. These findings indicate a growing vulnerability of the study area to extreme heat conditions and a clear deterioration in the thermal comfort of the area. Hence, the study area is progressively becoming susceptible to severe thermal conditions which adversely affect ecological life, therefore, there is an urgent need for appropriate mitigation measures. This outcome is consistent with the research findings of Kikon et al., [57] where extreme categories of thermal comfort index increased in areas with UHI.

Table 7
UHI statistics and corresponding ecological effects.

Year	Mean (μ)	Standard deviation (δ)	Threshold (°C) (μ + 0.5 × δ)	Non-UHI (0 < LST ≤ μ+ 0.5δ)		UHI (LST> μ + 0.5δ)	
				Area (km^2)	Area (%)	Area (km^2)	Area (%)
1991	24.6	1.11	25.16	141.25	73.70	50.45	26.30
2009	22.4	0.9	22.85	141.66	73.91	50.00	26.09
2016	22.9	1.24	23.52	118.17	61.66	73.49	38.34
2023	27.7	2.02	38.71	121.82	63.56	69.83	36.44

UTFVI	**Area (km^2)**				**Area (%)**				**UHI Effect**	**EEI**
	1991	**2009**	**2016**	**2023**	**1991**	**2009**	**2016**	**2023**		
<0.000	128.45	105.17	97.28	89.34	67.02	54.88	46.61	50.76	None	Excellent
0.000- 0.005	0.00	0.00	3.19	4.04	0.00	0.00	2.11	1.66	Weak	Good
0.005-0.010	0.00	19.35	3.34	4.29	0.00	10.10	2.24	1.74	Middle	Normal
0.010-0.015	12.80	0.00	3.42	4.62	6.68	0.00	2.41	1.78	Strong	Bad
0.015-0.20	0.00	0.00	3.56	5.34	0.00	0.00	2.78	1.86	Stronger	Worse
> 0.020	50.40	67.13	80.86	84.03	26.30	35.03	43.85	42.19	strongest	Worst

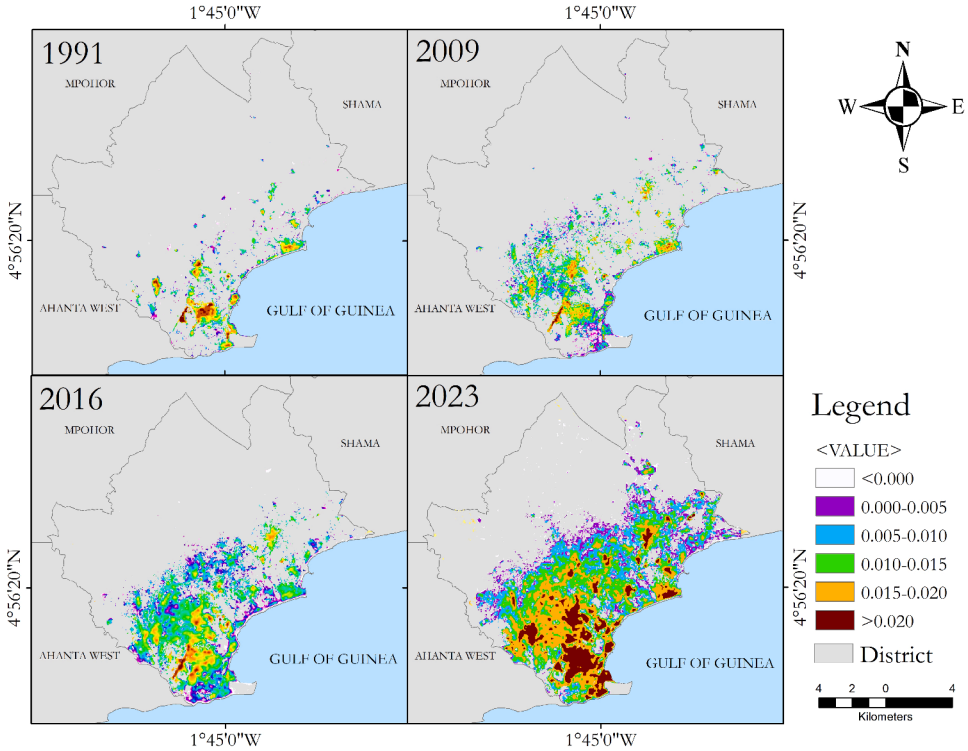

Fig. 10. UTFVI maps of the study.

Correlation of LST with land use indices

To examine the relationship between LST, NDBI, and NDVI, a correlation and linear regression analysis was employed. The regression analysis conducted for the years revealed a consistent positive correlation between LST and NDBI (Fig. 11). In 1991, the model exhibited a positive slope coefficient of 9.022x, indicating a significant positive influence of NDBI on LST, with an intercept value of 25.704. The coefficient of determination (R^2) of 0.6722 suggests that NDBI could explain 67.22 % of the variation in LST. Subsequently, this relationship was respectively strengthened in 2009, 2016, and 2023, with slope coefficients of 9.612x, 10.33x, and 11.69x, signifying an increasingly positive association between LST and NDBI. The intercept values for these years were 23.368, 23.82, and 28.58, respectively (Fig. 11). Furthermore, the R^2 values of 0.6973, 0.7784, and 0.8036 indicate that NDBI accounts for 69.73 %, 77.84 %, and 80.36 % of the variation in LST during the respective years. This temporal pattern suggests that the influence of built-up areas, as proxied by NDBI, on temperature patterns has become progressively more substantial, with NDBI emerging as an increasingly robust predictor of LST variations. Also, it highlights the significant impact of urbanized areas on surface temperature fluctuations, positioning them as primary drivers of the UHI phenomenon.

However, a contrasting relationship was revealed between LST and NDVI across the years. The regression models illustrated an inverse relationship between LST and NDVI, characterized by varying slopes and intercepts (Fig. 12). In 1991, the model exhibited a negative slope of -9.6332x, indicating a substantial influence of NDVI on LST, with an intercept of 27.311. Nonetheless, the R^2 value of 0.6428 suggests that approximately 64.28 % of the variability in LST can be attributed to NDVI. Also, in 2009, 2016, and 2023, the negative slopes of -8.2837x, -23.254x, and -20.409x respectively, showed a diminishing association between LST and NDVI. The intercepts of 2009, 2016, and 2023 were recorded as 22.813, 27.313, and 32.59, respectively (Fig. 12). Correspondingly, the R^2 values of 0.4364, 0.7465, and 0.7546 suggest that approximately 43.64 %, 74.65 %, and 75.46 % of the variability in LST can be explained by NDVI during these respective years. This suggests that NDVI influences temperature patterns within the metropolis. However, the limited variability of NDVI in explaining LST variations in 2009 suggests that other factors like urbanization, surface characteristics, and localized climate conditions might play a more significant role in governing LST fluctuations [13]. The corresponding correlation coefficient (r) for NDBI is 0.8199 for 1991, 0.8351 for 2009, 0.8823 for 2016, and 0.8964 for 2023 whereas NDVI were -0.80176 for 1991, -0.66058 for 2009, -0.81161 for 2016, and -0.86868 for 2023. Throughout the years, a positive correlation was observed between NDBI and LST while a negative correlation was observed between NDVI and LST. The direct correlation between NDBI and LST confirms the recognized concept that built-up areas contribute to elevated surface temperatures while the inverse relationship between NDVI and LST supports the established understanding that denser vegetation leads to cooler surfaces ([13,58]; Huang et al., 2024; [59, 60]).

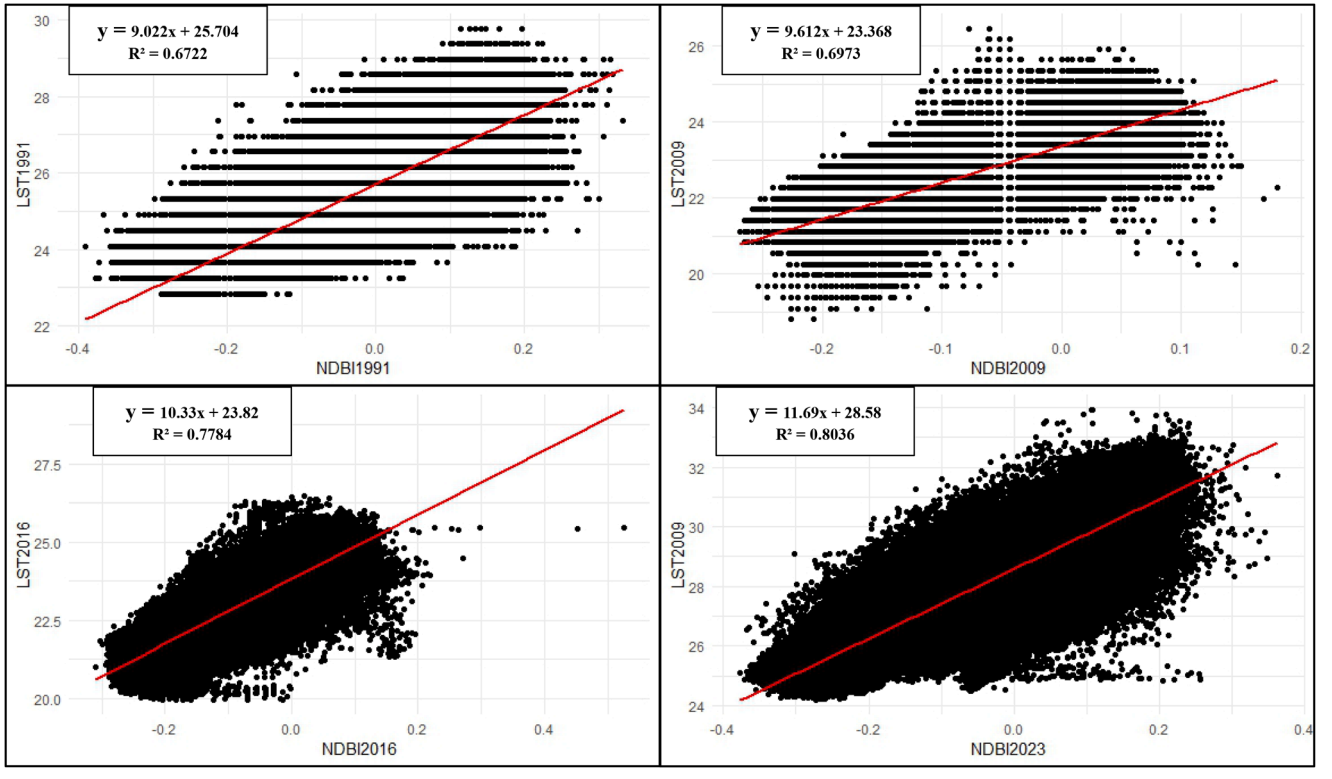

Fig. 11. Correlation between LST and NDBI.

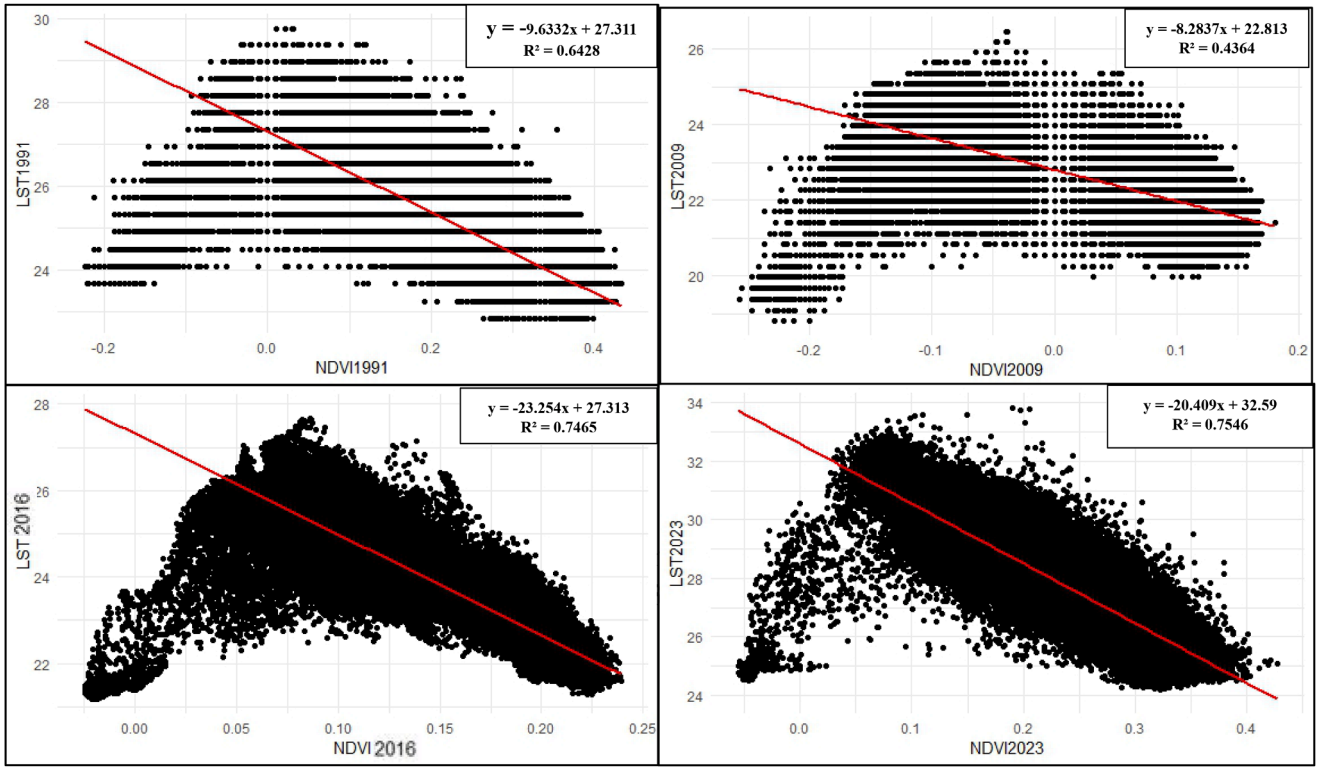

Fig. 12. correlation between LST and NDVI.

Table 8
LST values over different LULC categories.

LULC	LST (°C)											
	1991			2009			2016			2023		
	Mean	Min	Max	Mean	Min	Max	Mean	Min	Max	Mean	Min	Max
Water	25.67	23.67	28.98	21.36	18.81	24.81	20.94	19.94	24.71	26.44	24.48	32.90
Vegetation	24.47	22.84	28.98	22.24	19.97	26.47	22.54	20.17	26.47	26.48	24.19	32.63
Built-up	27.13	24.09	29.77	23.62	19.69	25.92	24.21	19.95	26.42	29.77	25.12	33.94

LULC	Change in LST(°C)					
	1991-2009	2009-2016	2016-2023	1991-2023	Yearly increase	Decadal increase
Water	-4.31	-0.42	5.50	0.76	0.02	0.24
Vegetation	-2.23	0.30	3.94	2.02	0.06	0.63
Built-up	-3.52	0.60	5.56	2.64	0.08	0.82

LST AND LC(LULC)

Land use land cover constitutes another significant parameter employed to examine the correlation between urbanization and its effects on the climate [13]. From Table 8, the average LST of each of the LULC increased over the study period. Water recorded the lowest LST while built-up had the highest LST.

Moreover, from 1991 to 2023 temperature increased at the rate of 0.76°C for water, 2.02°C for vegetation, and 2.64°C for built-up (Table 8). These temperature values for each land cover class revealed that the LST of the metropolis is significantly influenced by built-up. This finding is in agreement with the work of Shen et al., [61] where the highest LST was predominantly found in built-up areas while waterbodies and vegetation exhibited lower LST due to cooling effects. Also, similar results have been found by Mukherjee and Singh [60] in Surat and Bharuch cities in India and by Huda & Al, [25] in Chattogram City India where built-up class was identified as having the highest temperature as water experienced the lowest temperature. In Ghana, Wemegah et al., [20] found that LST in the greater Accra region exhibited higher values in built-up areas compared to areas covered by vegetation and water. Varied land cover types exhibit distinct biophysical characteristics, which influence their respective responses to solar radiation energy [62]. For instance, the absence of vegetation coupled with an increase in non-permeable surfaces leads to diminished latent heat fluxes and heightened sensible heat, consequently resulting in a noticeable warming effect. Waterbodies and vegetation have been discovered to significantly mitigate urban heat islands, therefore, incorporating them into urban planning and design of the metropolis can effectively regulate the thermal environment of the metropolis.

Conclusion

This study investigated the influence of urban growth on urban heat islands in the Sekondi-Takoradi metropolis from 1991 to 2023. LULC analysis revealed a significant shift in the land use from natural and undeveloped spaces to artificial and urbanized areas. These shifts were primarily driven by population growth and urbanization. Hence, contributing to environmental challenges such as water scarcity, loss of biodiversity, and influencing the thermal environment. Likewise, the increasing LST trend emphasizes a warming environment primarily affected by urban expansion and declining vegetation. The correlation between LST, NDBI, and NDVI unveiled the connection between urban expansion and increasing LST. Notably, the influence of built-up on temperature changes surpassed that of vegetation, emphasizing the crucial role of urbanization in temperature rise. Further, the UHI effect analysis showed that the city core and high-density areas registered higher temperatures than the low-density areas. Although this study offers a valuable understanding of the evolving urbanization, rising temperatures, and increasing urban heat island effects, it also highlights certain shortcomings and inadequacies. These are:

1. The remote sensing data employed were not able to capture details at the smallest scale due to its medium spatial resolution.
2. The study did not explore the distinct functions of vegetation types and green infrastructures to mitigate UHI effect.

These constraints not only highlight the necessity for careful interpretation of the results but also suggest potential avenues for future research. Also, the implementation of strategies such as rooftop gardening, green infrastructure, planned afforestation, and sustainability-focused policymaking and public awareness can help mitigate the impacts of UHI in the metropolis, thereby helping to achieve goal 11 of the sustainable development goals.

CRediT authorship contribution statement

Ernest Biney: Conceptualization, Formal analysis, Methodology, Writing – original draft, Writing – review & editing. **Eric Kwabena Forkuo:** Supervision, Writing – review & editing, Conceptualization. **Michael Poku-Boansi:** Supervision, Writing – review & editing. **Kwame O. Hackman:** Supervision, Software, Writing – review & editing. **Emmanuel Harris:** Writing – review & editing, Visualization. **Yaw Mensah Asare:** Methodology, Supervision, Writing – review & editing. **Daniel Buston Yankey:** Software,

Methodology, Visualization. **Ernestina Annan:** Writing – review & editing. **Albert Elikplim Agbenorhevi:** Writing – review & editing.

Declaration of competing interest

The authors declare that they have no known competing financial interests or personal relationships that could have appeared to influence the work reported in this paper.

Acknowledgments

My heartfelt gratitude goes to the Federal Ministry of Education and Research (BMBF) and the West African Science Centre on Climate Change and Adapted Land Use (WASCAL) for awarding me the scholarship that supported my PhD research, which led to the creation of this publication.

Declarations Ethical approval

All authors played a crucial role in shaping the concept of the study.

References

[1] C. Huang, Z. Zhou, M. Teng, C. Wu, P. Wang, Effects of climate, land use and land cover changes on soil loss in the Three Gorges Reservoir area, China, Geogr. Sustain. 1 (3) (2020) 200–208.
[2] H. Huang, J. Wang, C. Liu, L. Liang, C. Li, P. Gong, The migration of training samples towards dynamic global land cover mapping, ISPRS J. Photogramm. 161 (2020) 27–36, https://doi.org/10.1016/j.isprsjprs.2020.01.010.
[3] Kumi-boateng, B., & Stemn, E. (2015b). *Effect of Urban Growth on Urban Thermal Environment : A Case Study of Sekondi-Takoradi Metropolis of Ghana*. 5(2), 32–42.
[4] B. Halder, J. Bandyopadhyay, Evaluating the impact of climate change on urban environment using geospatial technologies in the planning area of Bilaspur, India, Environ. Challenges 5 (September) (2021) 100286, https://doi.org/10.1016/j.envc.2021.100286.
[5] A.S.K.N. Jumari, S. Kasniza, A. Najah, Y. Feng, J. Lin, C. Hoon, K. Lun, M. Sherif, A. Elshafie, Analysis of urban heat islands with landsat satellite images and GIS in Kuala Lumpur Metropolitan City, Heliyon 9 (8) (2023) e18424., https://doi.org/10.1016/j.heliyon.2023.e18424.
[6] M.B. Moisa, O.D. Gemeda, Assessment of urban thermal field variance index and thermal comfort level of Addis Ababa metropolitan city, Ethiopia, Heliyon 8 (8) (2022) e10185, https://doi.org/10.1016/j.heliyon.2022.e10185.
[7] R.R. Gyimah, C. Kwang, R.A. Antwi, E. Morgan Attua, A.B. Owusu, E.K. Doe, Trading greens for heated surfaces: Land surface temperature and perceived health risk in Greater Accra Metropolitan Area, Ghana, Egyptian J. Remote Sens. Space Sci. 26 (4) (2023) 861–880, https://doi.org/10.1016/j.ejrs.2023.09.004.
[8] V. Belenok, T. Noszczyk, L. Hebryn-baidy, S. Kryachok, Investigating anthropogenically transformed landscapes with remote sensing, Remote Sensing Appl.: Society and Environ 24 (September) (2021) 100635, https://doi.org/10.1016/j.rsase.2021.100635.
[9] D. Dutta, S. Gupta, A. Chakraborty, Effect of different land use land cover on surface heat budget – A case study from a tropical humid region of India, Remote Sens. Appl.: Soc. Environ. 25 (September 2021) (2022) 100675, https://doi.org/10.1016/j.rsase.2021.100675.
[10] A. Sekertekin, S. Bonafoni, Land Surface Temperature Retrieval from Landsat 5, 7, and 8 over Rural Areas : Assessment of Different Retrieval Algorithms and Emissivity Models and Toolbox Implementation, Remote. Sens. (2020).
[11] S. Rami, M. Alhaddad, A. Al-fugara, L. Al-hawwari, M. Al-hawwari, A. Omoush, M. Arar, Modeling the impact of urban land cover features and changes on the land surface temperature (LST): The case of Jordan, Ain Shams Eng. J. (2023) 102359, https://doi.org/10.1016/j.asej.2023.102359. *May*.
[12] A.K. Taloor, G. Parsad, S.F. Jabeen, M. Sharma, R. Choudhary, A. Kumar, Analytical study of land surface temperature for evaluation of UHI and UHS in the city of Chandigarh India, Remote Sens. Appl. Soc. Environ. 35 (April) (2024) 101206, https://doi.org/10.1016/j.rsase.2024.101206.
[13] U. Choudhury, S.K. Singh, A. Kumar, G. Meraj, P. Kumar, Assessing Land Use /Land cover changes and urban heat island intensification : a case study of kamrup metropolitan district, Northeast India (2000 –2032), Mdpi (2023) 503–521.
[14] S. Chatterjee, K. Gupta, Exploring the spatial pattern of urban heat island formation about land transformation : A study on a mining industrial region of West, Remote Sens. Appl.: Society and Environ. 23 (July) (2021) 100581, https://doi.org/10.1016/j.rsase.2021.100581.
[15] M. Zhao, H. Cai, Z. Qiao, X. Xu, Influence of urban expansion on the urban heat island effect in Shanghai, Int. J. Geogr. Inform. Sci. 30 (12) (2016) 2421–2441, https://doi.org/10.1080/13658816.2016.1178389.
[16] A. Al-Kafy, S. Rahman, A.-A. Faisal, M.M. Hassan, M. Islam, Modelling future land use land cover changes and their impacts on land surface temperatures in Rajshahi, Bangladesh, Remote Sensing Appl.: Society Environ. 18 (April) (2020) 100314, https://doi.org/10.1016/j.rsase.2020.100314.
[17] P. Mohammad, A. Goswami, S. Chauhan, S. Nayak, Urban Climate Machine learning algorithm based prediction of land use land cover and land surface temperature changes to characterize the surface urban heat island phenomena over Ahmedabad city , India, Urban Clim. 42 (2022) 101116, https://doi.org/10.1016/j.uclim.2022.101116.
[18] S. Guha, H. Govil, A. Dey, N. Gill, Analytical study of land surface temperature with NDVI and NDBI using Landsat 8 OLI and TIRS data in Florence and Naples city, Italy, European J. Remote Sensing 51 (1) (2018) 667–678, https://doi.org/10.1080/22797254.2018.1474494.
[19] M.B. Kursah, Urban Climate Satellite image analysis of thermal comfort for a sustainable urban ecology of Winneba, Ghana, Urban Climate 52 (January) (2023) 101685, https://doi.org/10.1016/j.uclim.2023.101685.
[20] C.S. Wemegah, E.I. Yamba, J.N.A. Aryee, F. Sam, L.K. Amekudzi, Assessment of urban heat island warming in the greater accra region, Scientific African 8 (2020) e00426, https://doi.org/10.1016/j.sciaf.2020.e00426.
[21] Ghana Statistical Service. (2021). *GHANA 2021 POPULATION AND HOUSING CENSUS*. 1–128.
[22] Service, G. S. (2014). *2010 Population and housing census report, Ghana Statistical Service*.
[23] E. Jahan, U. Rahman, Simulation of future land surface temperature under the scenario of climate change using remote sensing & GIS techniques of northwestern Rajshahi district, Bangladesh, Environ. Challenges 5 (October) (2021) 100365, https://doi.org/10.1016/j.envc.2021.100365.
[24] E. Stemn, B. Kumi, Modelling of land surface temperature changes as determinant of urban heat island and risk of heat - related conditions in the Wassa West Mining Area of Ghana, Modeling Earth Syst. Environ. (2020), https://doi.org/10.1007/s40808-020-00786-x. *0123456789*.
[25] N. Huda, A. Al, Assessment of urban thermal field variance index and defining the relationship between land cover and surface temperature in Chattogram city : A remote sensing and statistical approach, Environ. Challeng. 4 (March) (2021) 100107, https://doi.org/10.1016/j.envc.2021.100107.
[26] M. Chatwin, G. Arku, Co-creating an open government action plan: the case of Sekondi-Takoradi metropolitan assembly, Ghana, Growth Change 49 (2) (2018) 374–393, https://doi.org/10.1111/grow.12234.
[27] Ghana Statistical Service. (2014). *2010 POPULATION & HOUSING CENSUS REPORT*.
[28] Macrotrends (2024). Sekondi Takoradi, Ghana Metro Area Population 1950-2024. https://www.macrotrends.net/global-metrics/cities/21109/sekondi-takoradi/population. Retrieved January 10, 2024.

[29] Aduah, M. S., Mantey, S., & Area, T. M. (2020). *Modelling Potential Future Urban Land Use Changes in the Sekondi-Takoradi Metropolitan Area of Ghana*.
[30] STMA. (2022). *SEKONDI-TAKORADI METROPOLITAN ASSEMBLY MEDIUM-TERM DEVELOPMENT PLAN. June 2021*.
[31] O. Sarif, B. Rimal, E.N. Stork, Assessment of Changes in Land Use /Land Cover and Land Surface Temperatures and Their Impact on Surface Urban Heat Island Phenomena in the Kathmandu Valley (1988 –2018), Mdpi (2020) 29.
[32] M. Asif, J.H. Kazmi, A. Tariq, N. Zhao, R. Guluzade, W. Soufan, K.F. Almutairi, A.El Sabagh, M. Aslam, Modelling of land use and land cover changes and prediction using CA-Markov and Random Forest, Geocarto Int. 38 (1) (2023), https://doi.org/10.1080/10106049.2023.2210532.
[33] P. Lukas, A.M. Melesse, T.T. Kenea, Prediction of Future Land Use / Land Cover Changes Using a Coupled CA-ANN Model in the Upper Omo – Gibe River, 2023.
[34] M. Fernández-Delgado, Do we need hundreds of classifiers to solve real world classification problems? J. Mach. Learn. Res. 15 (1) (2014) 3133–3181.
[35] D. Hidalgo-García, J. Arco-Díaz, Modeling the Surface Urban Heat Island (SUHI) to study of its relationship with variations in the thermal field and with the indices of land use in the metropolitan area of Granada (Spain), Sustainable Cities and Society 87 (May) (2022), https://doi.org/10.1016/j.scs.2022.104166.
[36] X. Xiang, C. Qiu, J. Hu, Y. Shi, Y. Wang, M. Schmitt, H. Taubenb, The urban morphology on our planet – global perspectives from space, Remote Sens. Environ. 269 (September 2021) (2022) 1–11, https://doi.org/10.1016/j.rse.2021.112794.
[37] N.R. Khwarahm, P.R. Najmaddin, K. Ararat, S. Qader, Past and future prediction of land cover land use change based on earth observation data by the CA – Markov model : a case study from Duhok governorate, Iraq, Arabian J. Geosciences, Springer (2021) 1–14.
[38] Wangyel, S., Munkhnasan, L., & Lee, W. (2021). *Land use and land cover change detection and prediction in Bhutan ' s high altitude city of Thimphu, using cellular automata and Markov chain. 2*(November 2020). https://doi.org/10.1016/j.envc.2020.100017.
[39] R. Khan, H. Li, M. Basir, Y. Lin, Monitoring land use land cover changes and its impacts on land surface temperature over Mardan and Charsadda Districts, Khyber Pakhtunkhwa (KP), Pakistan, Environ. Monit. Assess. (2022), https://doi.org/10.1007/s10661-022-10072-1. *May*.
[40] M. Shamsudeen, R. Padmanaban, P. Cabral, P. Morgado, Spatio-Temporal Analysis of the Impact of Landscape Changes on Vegetation and Land Surface Temperature over Tamil Nadu, MDPI 3 (2022) 614–638.
[41] S. Guha, Dynamic seasonal analysis on LST-NDVI relationship and ecological health of Raipur City, India, Ecosystem Health and Sustainability 7 (1) (2021) 1–13, https://doi.org/10.1080/20964129.2021.1927852.
[42] Al-khakani, E. T. (2023). *Land Surface Temperature Dynamics in Response to Changes in Land Cover in An-Najaf Province, Iraq. July*. https://doi.org/10.7780/kjrs.2023.39.1.7.
[43] S. Guha, Dynamic analysis and ecological evaluation of urban heat islands in Raipur city, India, J. Appl. Remote Sens. 11 (03) (2017) 1, https://doi.org/10.1117/1.jrs.11.036020.
[44] J.D. Osei, P. Damoah-Afari, L.L. Yevugah, C. Mensah, N.A. Prempeh, Impact of land use and land cover dynamics on urban heat island in the Sunyani Municipality using satellite remote sensing, J. Ghana Institution of Eng. (JGhIE) 23 (2) (2023) 6–16, https://doi.org/10.56049/jghie.v23i2.61.
[45] H. Saleem, R. Ahmed, S. Mushtaq, S. Saleem, Remote sensing-based analysis of land use, land cover, and land surface temperature changes in Jammu District, India, Int. J. River Basin Manage. (2024) 1–16, https://doi.org/10.1080/15715124.2024.2327493. *March*.
[46] C.A. Mensah, J.K. Eshun, Y. Asamoah, E. Ofori, Changing land use /cover of Ghana ' s oil city (Sekondi-Takoradi Metropolis): implications for sustainable urban development, Int. J. Urban Sustainable Develop. 11 (2) (2019) 223–233, https://doi.org/10.1080/19463138.2019.1615492.
[47] E. Biney, E.K. Forkuo, M. Poku-Boansi, Y.M. Asare, K.O. Hackman, D.B. Yankey, A.E. Agbenorhevi, E. Annan, A comprehensive analysis and future projection of land use and land cover dynamics in a fast-growing city: A case study of Sekondi-Takoradi metropolis, Ghana, Scientific African 24 (February) (2024) e02207, https://doi.org/10.1016/j.sciaf.2024.e02207.
[48] E. Dadzie-paintsil, J.V. Mensah, Effects of urbanization on coastal wetlands in the Sekondi-Takoradi Metropolis, Ghana 6 (2) (2022) 94–105, https://doi.org/10.13057/oceanlife/o060205.
[49] Tasantab, J. (2019). *Beyond the plan : How land use control practices influence flood risk in Sekondi-Takoradi*. 1–9.
[50] Asare, Y. M., Selby, I., Ashiagbor, G., & Asante, C. Y. (2023). *Analysis and prediction of land use land cover dynamics in the Kpeshie Lagoon Basin of Ghana using satellite remote sensing*.
[51] E. Biney, E. Boakye, Urban sprawl and its impact on land use land cover dynamics of Sekondi-Takoradi metropolitan assembly, Ghana, Environmental Challenges 4 (April) (2021) 100168, https://doi.org/10.1016/j.envc.2021.100168.
[52] Obeng, K., Forkuo, E. K., Asare, Y. M., Opoku, P., & Obeng, A. S. (2023). *Land Use Land Cover Changes in the Densu River Basin of Ghana From 1991 To 2020*. 41 (1), 1–18.
[53] K. Frimpong, D. Eugene, E.J.Van Etten, Urban sprawl and microclimate in the Ga East municipality of Ghana, Heliyon 8 (March) (2022) 09791, https://doi.org/10.1016/j.heliyon.2022.e09791.
[54] G. Rasul, A. Mahmood, A. Sadiq, S.I. Khan, Vulnerability of the Indus Delta to cli- mate change in Pakistan, Pak. J. Meteorol. 8 (16) (2012).
[55] M. Badasa, B. Temesgen, L. Busha, I. Niguse, D. Obsi, Analysis of land surface temperature using Geospatial technologies in Gida Kiremu, Limu, and Amuru District, Western Ethiopia, Artificial Intell. Agriculture 6 (2022) 90–99, https://doi.org/10.1016/j.aiia.2022.06.002.
[56] A.M. Siddique, F. Boqing, L. Dongyun, Modeling the Impact and Risk Assessment of Urbanization on Urban Heat Island and Thermal Comfort Level of Beijing City, China (2005–2020), Sustainability (Switzerland) 15 (7) (2023), https://doi.org/10.3390/su15076043.
[57] N. Kikon, D. Kumar, S.A. Ahmed, Quantitative assessment of land surface temperature and vegetation indices on a kilometer grid scale, Environ. Science and Pollution Res. 30 (49) (2023) 107236–107258, https://doi.org/10.1007/s11356-023-27418-y.
[58] D.B. Cevik, M. Cetin, Evaluation of UTFVI index effect on climate change in terms of urbanization, Environ. Sci. Pollution Res. 30 (30) (2023) 75273–75280, https://doi.org/10.1007/s11356-023-27613-x.
[59] A. Mondal, S. Guha, S. Kundu, Dynamic status of land surface temperature and spectral indices in Imphal city, India from 1991 to 2021, Geomatics, Natural Hazards and Risk 12 (1) (2021) 3265–3286, https://doi.org/10.1080/19475705.2021.2008023.
[60] F. Mukherjee, D. Singh, Assessing Land Use – Land cover change and its impact on land surface temperature using LANDSAT Data : a comparison of two Urban Areas in India, Earth Systems Environ. (2020), https://doi.org/10.1007/s41748-020-00155-9. *0123456789*.
[61] C. Shen, H. Hou, Y. Zheng, Y. Murayama, R. Wang, T. Hu, Prediction of the future urban heat island intensity and distribution based on landscape composition and configuration: A case study in Hangzhou, Sustainable Cities and Society 83 (2318) (2022) 103992, https://doi.org/10.1016/j.scs.2022.103992.
[62] L. Tian, Y. Tao, M. Li, C. Qian, T. Li, Y. Wu, Prediction of land surface temperature considering future land use change effects under climate change scenarios in Nanjing City, China, Remote Sens. 15 (11) (2023) 2914.